




# Thermal/fluid characteristics of the inline stacked plain-weave screen as solar-powered Stirling engine heat regenerators

Hamed Mortazavi<sup>1</sup>  | Hamidreza Mortazavy Beni<sup>1</sup>  | Mohammad Saidul Islam<sup>2</sup> 

<sup>1</sup> Department of Biomedical Engineering, Arsanjan Branch, Islamic Azad University, Arsanjan, Iran

<sup>2</sup> School of Mechanical and Mechatronic Engineering, University of Technology Sydney (UTS), Ultimo, Australia

## Correspondence

Hamidreza Mortazavy Beni, Department of Biomedical Engineering, Arsanjan Branch, Islamic Azad University, Arsanjan, Iran.

Email: [h.mortazavy@iaua.ac.ir](mailto:h.mortazavy@iaua.ac.ir); [h.mortazavy@gmail.com](mailto:h.mortazavy@gmail.com)

## Funding information

Teb Karan Aran Far Company; National Talent Sponsorship, Grant/Award Number: RS990431

## Abstract

The present work demonstrates the results of a 3D numerical analysis of heat transfer and fluid flow through a fabricated aluminium wire filament, bonded mesh deployed as a regenerator surface in the Stirling engine. Here, two inline regenerator models with the same mass but different geometry were simulated by computational fluid dynamics (CFD) and finite element method (FEM). The results show that the temperature efficiency of both inline with non-uniform and uniform wire diameters is almost equal. However, the non-uniform diameter model is shorter and reaches the maximum thermal efficiency faster in reduced length  $< 18$ . Also, it shows approximately 5% a greater mean thermal efficiency. In general, from this simulation, it can be seen that changes in the geometry of the heat regenerator can have a direct effect on thermal efficiency and pressure drop in the same mass. Therefore, using the inline stacked plain-weave screen with a non-uniform wire diameter regenerator in the powered Stirling engine is recommended due to space constraints. Small changes in the regenerator geometry lead to immense leaps in increasing a solar power plant's overall efficiency.

## 1 | INTRODUCTION

A regenerative heat exchanger, or more commonly a regenerator, is a heat exchanger where heat from the hot fluid is intermittently stored in a thermal storage medium before it is transferred to the cold fluid. The hot fluid is brought into contact with the heat storage medium, and then the fluid is displaced with the cold fluid, which absorbs the heat [1]. In this regard, woven mesh structures are used as heat exchangers and thermal regenerators in many industrial applications, including solar energy collection, interagency plans to develop an artificial heart, aerospace, Stirling engines, food processing, heat recovery, heat pipe systems, and others [2]. The most important features of these structures are their flow pressure drop characteristics and thermal performance [3]. Such effects, however, are functions of many geometrical, thermal, and fluid hydrodynamical parameters. Therefore, due to a large number of these parameters, numerical analysis is inevitable for heat regenerator design with wire screen structures [4]. Considering the growing environmental issues, renewable energy converters such as solar cogeneration systems have received more attention during

recent years. Solar cogeneration systems convert the thermal energy of solar radiation into mechanical energy (utilizing a Stirling engine) and then into electrical power (using a linear generator) [5]. Tong and London [6] reported friction factor and heat transfer coefficient measurements for air flowing through inline plain-weave screen laminates and staggered cross-rod matrices. Kays and London [7] have pointed out that the most effective way to increase a heat exchanger's performance is to increase its surface area to volume ratio. Small-particle packed beds, and foamed metals are expanded materials having a large surface area to volume ratio values. However, due to the tortuosity effect in conjunction with these materials' high porosity, their effective thermal conductivity is relatively small. Much of the gain in performance obtained by having a large area to volume ratio is lost by having a relatively small effective thermal conductivity. Typical thermal conductivity values in fused-particle packed beds are 10–15% of the particle thermal conductivity. Xu and Wirtz [8] developed a model for the in-plane effective thermal conductivity of screen-laminates. They showed that these structures could be configured to have a large surface area to volume ratio, and high effective thermal

This is an open access article under the terms of the [Creative Commons Attribution-NonCommercial-NoDerivs](https://creativecommons.org/licenses/by-nc-nd/4.0/) License, which permits use and distribution in any medium, provided the original work is properly cited, the use is non-commercial and no modifications or adaptations are made.

© 2022 The Authors. *IET Renewable Power Generation* published by John Wiley & Sons Ltd on behalf of The Institution of Engineering and Technology

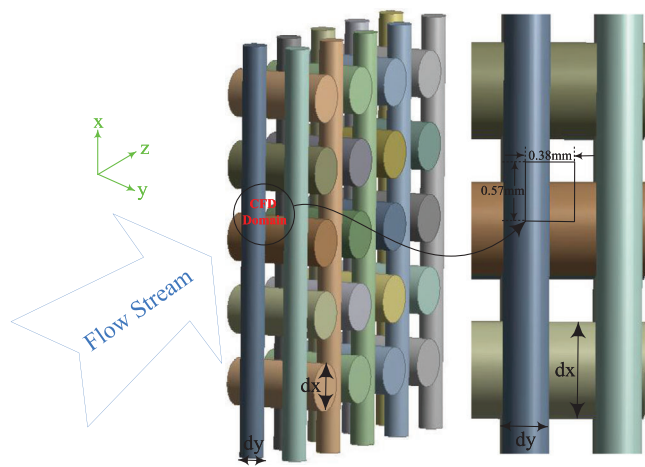


**FIGURE 1** 3D orthogonal plain-weave in-line with non-uniform wire diameter screen laminates ( $dx = 0.76$  mm,  $dy = dx/2 = 0.38$  mm)

conductivity in a particular direction with effective thermal conductivities of anisotropic screen laminates approaching 78% of base material values. Park et al. [9] developed a two-energy equation model for heat transfer in thin porous media. They considered chilled water flow through in-line and staggered isotropic plain-weave screen laminates. They measured friction factors and Colburn  $j$ -factors similar to those measured by Tong and London. They found that screen-laminate based heat exchange matrices could be configured to have pressure-drop and thermal performance superior to fused particle bed exchange matrices having the same mass per volume. Wirtz and Xu [10] demonstrated a 3D fabrication methodology, aluminium wire filament, and bonded mesh deployed as a heat exchange surface. They found that the weaving wire bonding process must be carefully controlled to ensure that target porosity, specific surface area and effective thermal conductivity are achieved. Also, Faruoli et al. [11] investigated a numerical study to simulate a porous matrix to use it as a heat exchanger. In this study, the solid part of the numerical domain is considered the region with the highest porosity. The results indicate that the amount of friction coefficient decreases with increasing Reynolds number. Because the porous media's geometry within the regenerator is incredibly complex, it is essential to provide an accurate model of how heat is transferred. In this regard, wired models in terms of heat transfer show better behaviour than other models with angular cross-sections, including rectangular. In general, the optimal wire filaments arrangement can be advantageous in heat regenerators' performance to achieve the desired thermal efficiency [12]. In the present work, the thermal efficiency and the pressure drop across a woven mesh structure similar to that introduced by Figure 1 are investigated numerically.

## 2 | METHODS

Figure 2 shows an inline heat regenerator. Figure 2I designed model consists of fifteen filaments of an aluminium wire joined in an orthogonal geometry. According to Figure 2I, the hori-

zontal wires are seven filaments, and vertical wires are eight filaments. Figure 2II designed model consists of thirty-two filament of an aluminium wire that is joined to each other in an orthogonal geometry with the same diameter (0.38 mm) so that its mass is the same as the Figure 2I. Due to symmetry, only a small part of the regenerator is considered. The selected computational cell is 0.38 mm $\times$ 0.57 mm (Figures 1 and 3). Figure 3 shows a hybrid unstructured grid mesh generation for fluid and solid domain with the hybrid tetrahedral and hexahedral elements. The meshes shown in this image have been selected coarse mesh than the software environment for the sample shown. Also, especially at the wires' contact points, the number of meshes has been selected finer to better consist of the boundary layer and fluid-solid heat transfer interface. AutoCAD Mechanical 2021(x64) software was employed for building the geometrical structure. Also, ANSYS 2020 R1 packages are used for grid generation in the design modeler and solver software. The total number of elements for regenerator of Figure 3I provided 63,048 and for Figure 3II up to 87,929 computational cells after grid independency.

## 3 | GOVERNING EQUATION AND BOUNDARY CONDITION

The continuity and momentum equations for air as viscous and incompressible unsteady working gas flow can be written as follows [13]:

$$\frac{\partial U_i}{\partial x_i} = 0 \quad (1)$$

$$\begin{aligned} & \rho \left( \frac{\partial U_i}{\partial t} + U_i \frac{\partial U_j}{\partial x_j} \right) \\ & = -\frac{\partial P}{\partial x_i} + \frac{\partial}{\partial x_j} \left[ \mu \left( \frac{\partial U_i}{\partial x_j} + \frac{\partial U_j}{\partial x_i} \right) - \left( \frac{2}{3} \delta_{ij} \frac{\partial U_k}{\partial x_k} - \rho \overline{U_i' U_j'} \right) \right] + G_i \end{aligned} \quad (2)$$

In these equations, the parameters  $U$ ,  $\rho$ ,  $P$ ,  $\mu$ ,  $\delta_{ij}$ , and  $G_i$  for air-fluid represent velocity, density, static pressure, fluid dynamic viscosity, Kronecker delta, and gravity term, respectively. Also,  $i$  and  $j$  represent Cartesian coordinates.  $\rho \overline{U_i' U_j'}$  is Reynolds stresses. It is additional in Equation (2) momentum fluxes due to the transient turbulent motion. The energy equation is in the following form [14]:

$$\begin{aligned} & \frac{\partial}{\partial t} (\rho E) + \nabla \cdot (\vec{V} (\rho E + p)) \\ & = \nabla \cdot (k_{eff} \nabla T - \sum_j h_j \vec{J}_j + (\vec{\tau}_{eff} \cdot \vec{V})) \end{aligned} \quad (3)$$

$$k_{eff} = k + k_t \quad (4)$$

where  $\vec{V}$ ,  $k_{eff}$ ,  $k$ ,  $k_t$ ,  $\vec{J}_j$ , and  $\vec{\tau}_{eff}$  are the overall velocity vector, effective conductivity, thermal conductivity, the turbulent

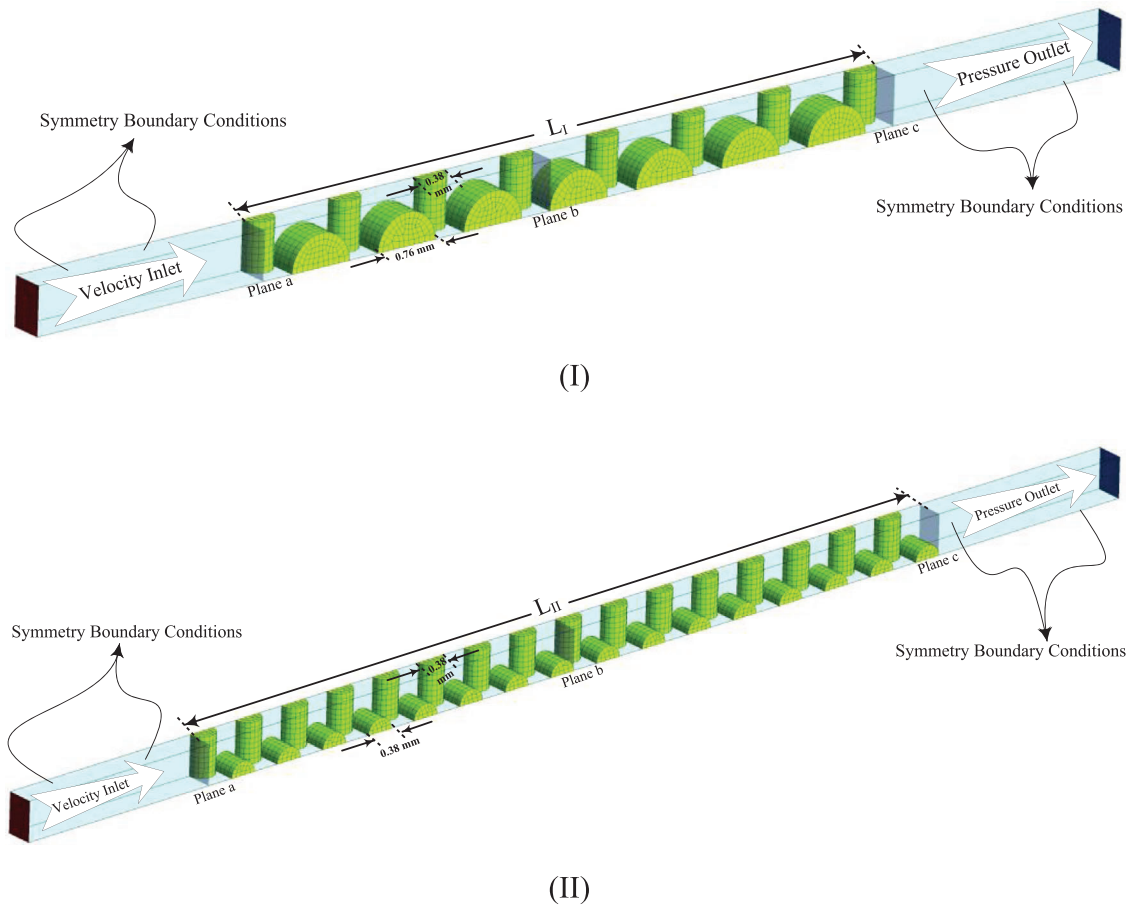


**FIGURE 2** Computational domain for an inline heat regenerator. (I) Non-uniform inline regenerator: Non-uniform wire diameter ( $L_I = 8.36$  mm,  $\varepsilon_I = 0.48$ ). (II) Uniform inline regenerator: Uniform wire diameter ( $L_{II} = 12.16$  mm,  $\varepsilon_{II} = 0.33$ )

thermal conductivity, the diffusion flux of species  $j$ , and stress tensor, respectively.  $k_{eff} \nabla T$ ,  $\sum_j b_j \vec{J}_j$ , and  $\vec{\tau}_{eff} \vec{V}$  represent energy transfer due to conduction, species diffusion, and viscous dissipation, respectively. The airflow on the aluminium wires is turbulent. The RNG  $k - \varepsilon$  turbulence model was used to solve the turbulent flow. This viscous simulation used a differential viscosity model with enhanced wall treatment. Also, pressure gradient and thermal effects options were considered in the solver software. As shown in Figure 2, the symmetry boundary conditions are considered for sidewalls of the domain. On the other hand, input with velocity inlet and output with pressure outlet boundary condition is selected. Also, for the Air-solid contact surface, the fluid–solid heat transfer interface with thermally coupled conditions is activated. Oscillating flow user-defined function (UDF) is used for velocity inlet boundary conditions. Inlet flow velocity is considered to obey the following equation:

$$V = V_{max} \sin \omega t \quad (5)$$

Where  $V_{max} = 2$  m/s is velocity amplitude, and  $\omega = 10$  rad/s is angular velocity. Therefore, the heating and cooling time is

equal to  $t_b = t_c = \frac{\pi}{10}$  s. The flow is unsteady and for solution chosen time step  $= \frac{\pi}{1000}$  s. The hot air inlet temperature is taken to be 900 K, and the cold air temperature is 400 K [15].

## 4 | RESULTS

For validation, the friction factor ( $f$ ) of two inline heat exchanger models presented by Tong and London [6] and Park et al. [9] is used, as shown in Figure 4. As can be seen from this figure, the deviation from the laboratory results is less than 5%. The friction factor and the Reynolds number ( $R_e$ ) are defined based on the channel hydraulic diameter ( $D_b$ ) as:

$$D_b = \frac{4A_a}{P_a} \quad (6)$$

$$R_e = \frac{\rho_f V D_b}{\mu} \quad (7)$$

$$\frac{\Delta P}{\rho_f} = f \frac{L}{D_b} \frac{V^2}{2} \quad (8)$$

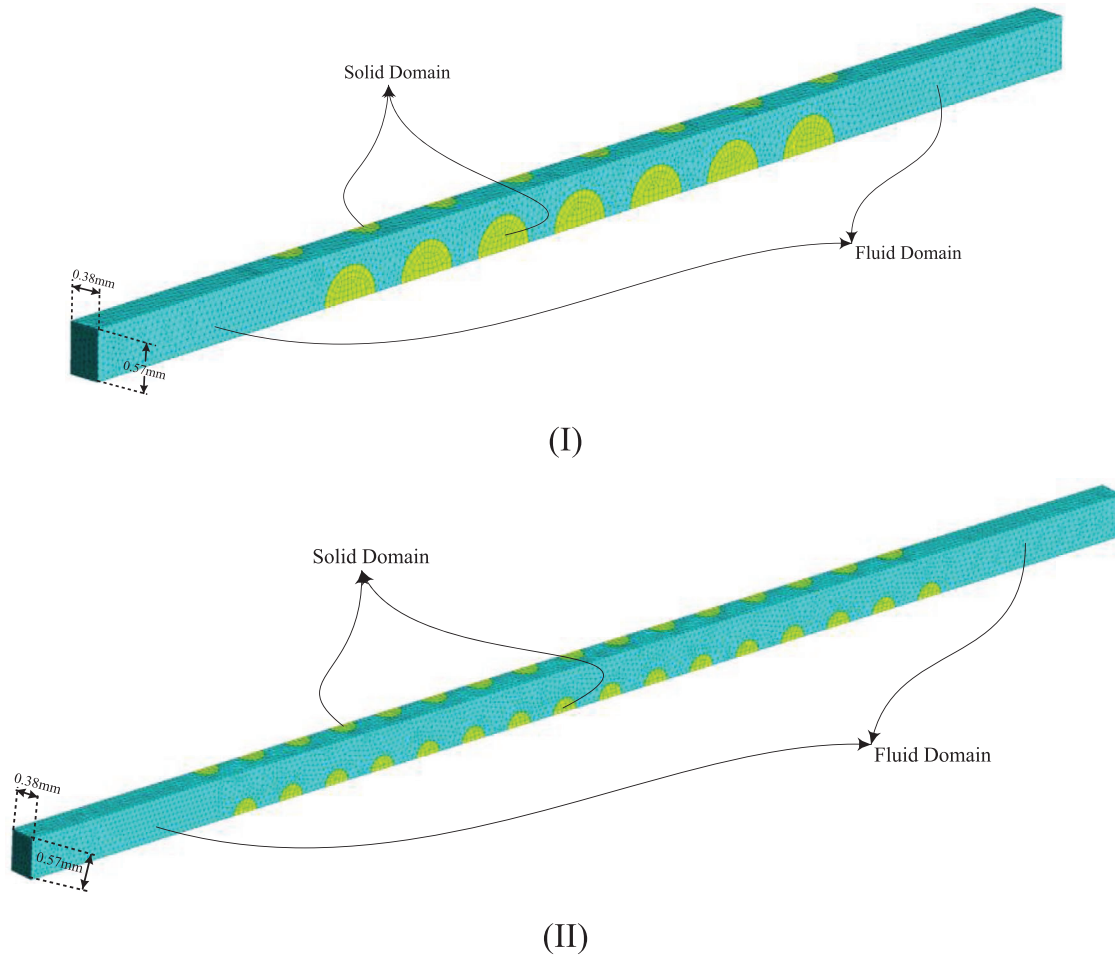


**FIGURE 3** Numerical mesh domain for an inline heat regenerator. (I) Non-uniform inline regenerator. (II) Uniform inline regenerator

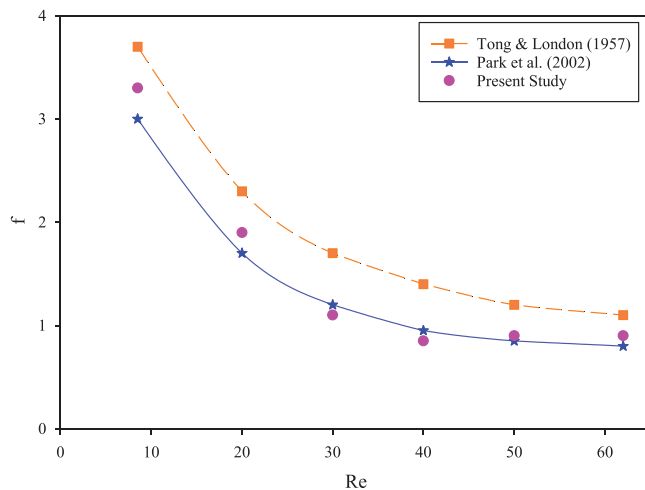


**FIGURE 4** Frictional factor versus Reynolds number for comparison between experimental data and numerical simulation

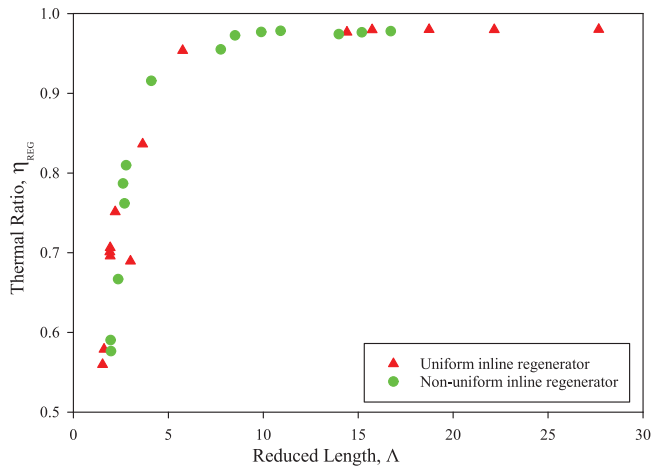
Where In these relationships  $A_w$ ,  $P_w$ ,  $\rho_f$ ,  $\Delta P$ , and  $L$  are a cross-sectional area of the flow, the wetted perimeter of the cross-section, fluid density, pressure drop, and regenerator length, respectively.

After the heating and cooling period of the heat regenerator in the software was repeated so much that the regenerator reached energy equilibrium; thermal efficiency ( $\eta_{REG}$ ) in terms of reduced length ( $\Lambda$ ) can be calculated as follows [15]:

$$\Lambda = \frac{bA}{\dot{m}_f c_f} \quad (9)$$

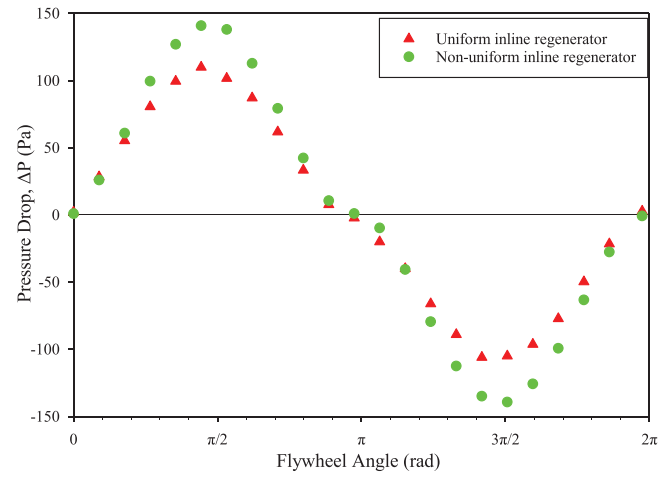
$$\eta_{REG} = \frac{T_{fb, in} - T_{fb, out}}{T_{fb, in} - T_{fc, in}} \quad (10)$$

Where in these relationships  $b$ ,  $A$ ,  $\dot{m}_f$ ,  $c_f$ , and  $T$  are wire heat transfer coefficient, regenerator matrix heat transfer surface area, mass flow rate, airflow specific heat at constant pressure, and temperature, respectively. In Figure 5, the thermal efficiency of the regenerators versus reduced length is shown. The trend of thermal efficiency changes versus reduced length is the same for both models; only the speed of reaching the maximum efficiency in the non-uniform is higher than the uniform inline regenerator. In other words, it can be seen that the thermal efficiency of the uniform and non-uniform inline regenerator could be reached to 98 % efficiency at 10 and 15 reduced lengths, respectively.



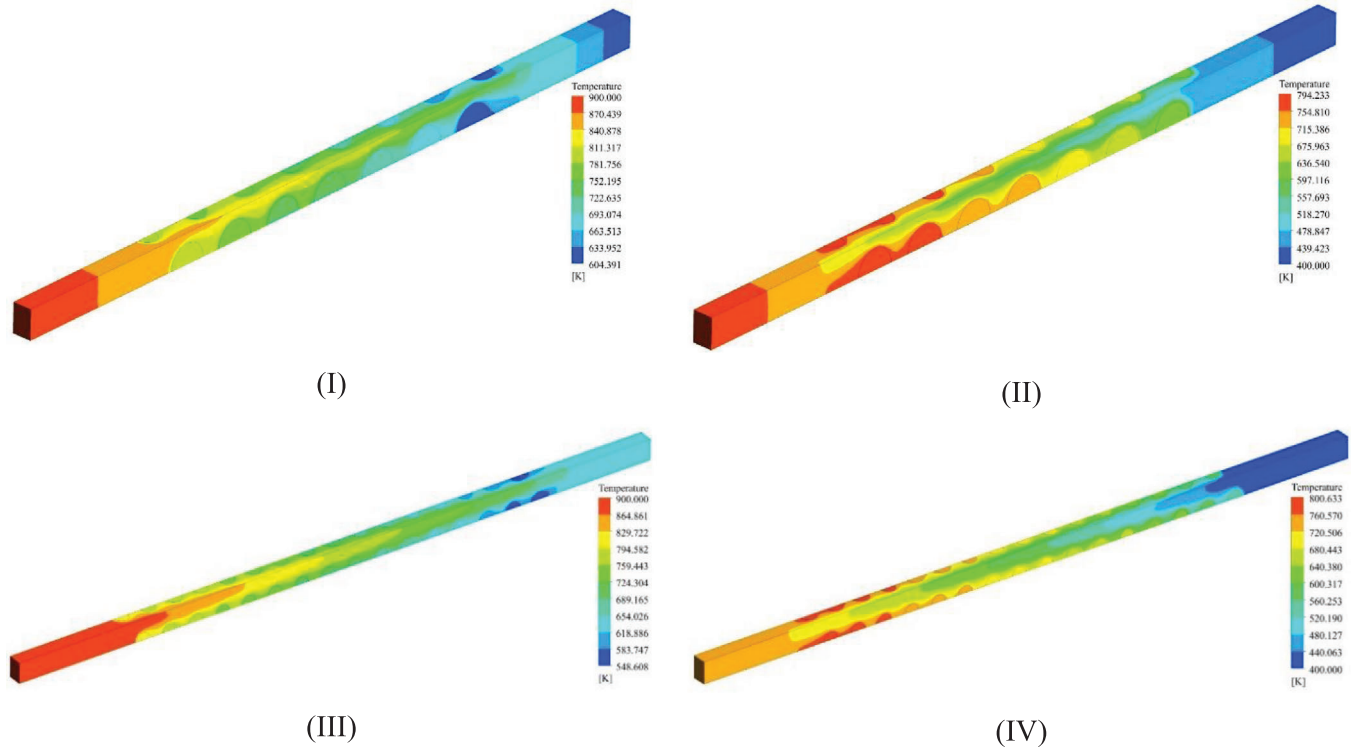
**FIGURE 5** The thermal efficiency of heat regenerators versus reduced length for non-uniform and uniform inline regenerators

Figure 6 shows the temperature contour for the case where  $\omega = 10 \text{ rad/s}$  and  $V_{max} = 2 \text{ m/s}$  at flywheel angle  $\frac{\pi}{2}$  and  $\frac{3\pi}{2}$  in a heating and cooling period, respectively. Comparison of temperature counters in Figure 6I and Figure 6III shows that the non-uniform inline regenerator has three wires, and the uniform inline regenerator has six wires at the end of the regenerator in the temperature lower than 650 K at heating period. Also, by comparing Figure 6II and Figure 6IV, it can be seen that non-uniform inline regenerator has eight wires and uniform inline



**FIGURE 7** The pressure drop of heat regenerator versus flywheel angle for non-uniform and uniform inline regenerators

regenerator has thirteen wires at the end of the regenerator in the temperature higher than 700 K at cooling period. For better recovery performance, more heat must be absorbed in the end wires of the regenerator in the heating period. Also, more heat must be released from the end wires of the regenerator in the cooling period. Figure 7 shows the mean pressure drop for the two models presented. According to Figure 7, the regenerator with non-uniform exhibits more pressure drop relative to the uniform inline regenerator. The minimum pressure drop is



**FIGURE 6** The temperature contour at  $\omega = 10 \text{ rad/s}$  and  $V_{max} = 2 \text{ m/s}$  at flywheel angle  $\frac{\pi}{2}$  and  $\frac{3\pi}{2}$  in a heating and cooling period, respectively. (I) Heating period for non-uniform inline regenerator. (II) Cooling period for non-uniform inline regenerator. (III) Heating period for uniform inline regenerator. (IV) Cooling period for uniform inline regenerator

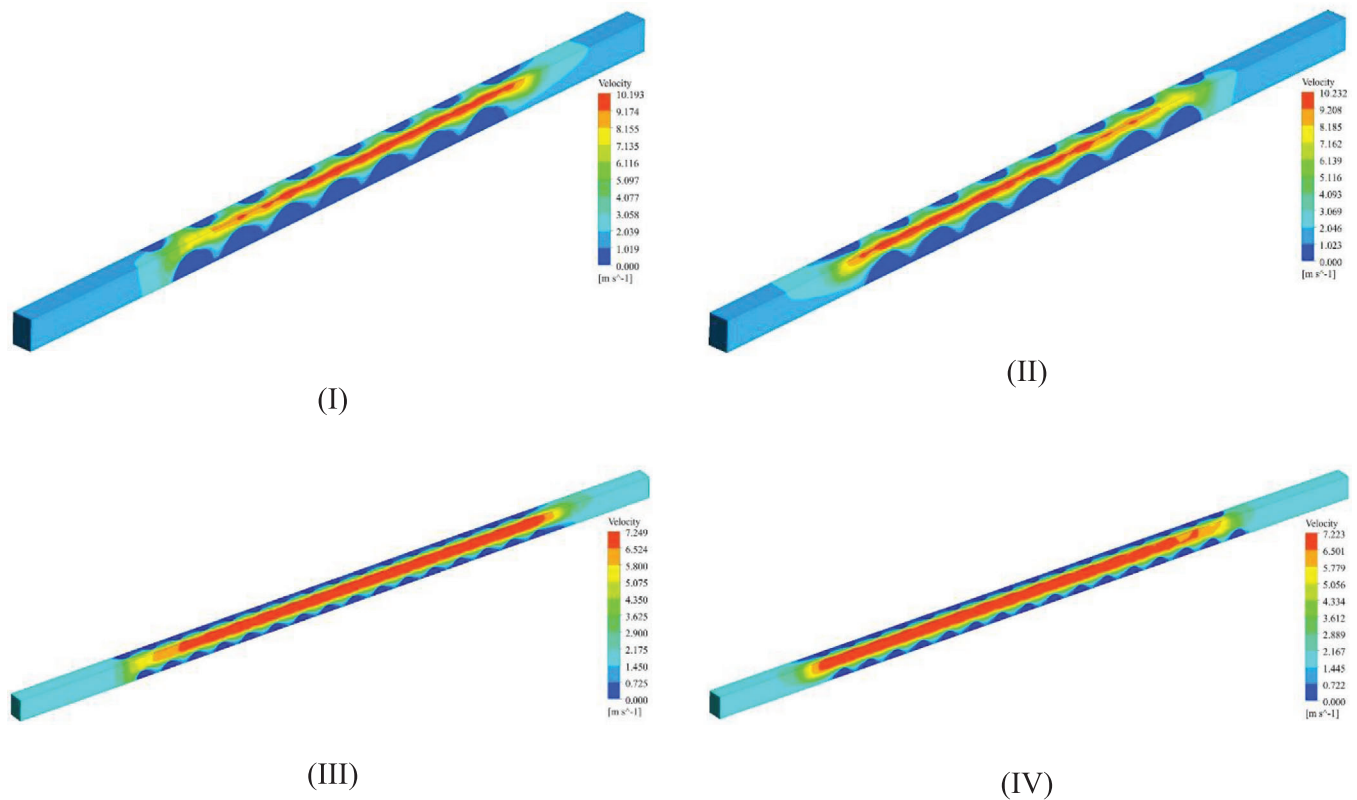


**FIGURE 8** The velocity contour at  $\omega = 10$  rad/s and  $V_{max} = 2$  m/s at flywheel angle  $\frac{\pi}{2}$  and  $\frac{3\pi}{2}$  in a heating and cooling period, respectively. (I) Heating period for non-uniform inline regenerator. (II) Cooling period for non-uniform inline regenerator. (III) Heating period for uniform inline regenerator. (IV) Cooling period for uniform inline regenerator

0 Pa. It achieved at the beginning of the heating and cooling periods (0,  $\beta$ ). Also, subtraction of the maximum pressure drop between regenerators was achieved at the middling of the heating and cooling periods ( $\frac{\pi}{2}, \frac{3\pi}{2}$ ), which is approximately equal to 30 Pa.

Velocity contours for each of the heat regenerators are shown in Figure 8. The trend of velocity changes is the same in non-uniform and uniform inline regenerators with different quantities. In the central path of fluid motion through the tissue of the wire filaments, the most significant increase in velocity occurs due to narrowing the path of fluid motion. The instantaneous velocity can then increase in the centre line of movement in non-uniform and uniform inline regenerators to 5 and 3.5 times the inlet velocity, respectively.

## 5 | DISCUSSION

The use of heat regenerators to prevent heat loss of the solar-powered Stirling engine has always been considered by researchers [16–18], among which inline stacked plain-weave screen regenerators due to the more straightforward structure to build and lower pressure drop, have received more attention [8–10]. In this study, with the help of the proportional numerical calculation method and using High-Performance Computing Research Center (HPCRC), the validation of numerical and laboratory results with a low deviation was achieved (Figure 4).

It should be noted that in order for the regenerator to reach thermal equilibrium, the number of iterations needs to be several hundred thousand times (Figure 9), which takes time to get the final results. In general, CFD analysis is an efficient and powerful tool for modeling and investigating other domains in different critical locations [19–23]. The Stirling cycle is a thermodynamic cycle that transforms thermal energy into mechanical energy. A key component of Stirling engines is the regenerator, which stores and releases thermal energy periodically. The existence of a regenerator raises the efficiency of the engine by maintaining heat within the system that otherwise would be exchanged with the environment. It reduces the heat flow from the high-temperature reservoir to the low-temperature reservoir without any additional gain of mechanical work [24]. Generally, various bonded mesh deployed as a regenerator surface is utilized to fabricate heat recovery, but most of them have straightforward geometries [25]. To some extent, the bonded mesh designed based on these geometries can recover the heat produced by regenerative systems [26]. However, there is still the thermal efficiency and pressure drop problem in wire filament surfaces due to space constraints to installation [27].

This comparison of temperature efficiency occurs while the mass of two identical regenerators is selected the same, and only the essential role is played by the effect of the regenerator's geometry. According to Figure 5, the non-uniform inline regenerator can achieve 97% efficiency during lower reduced

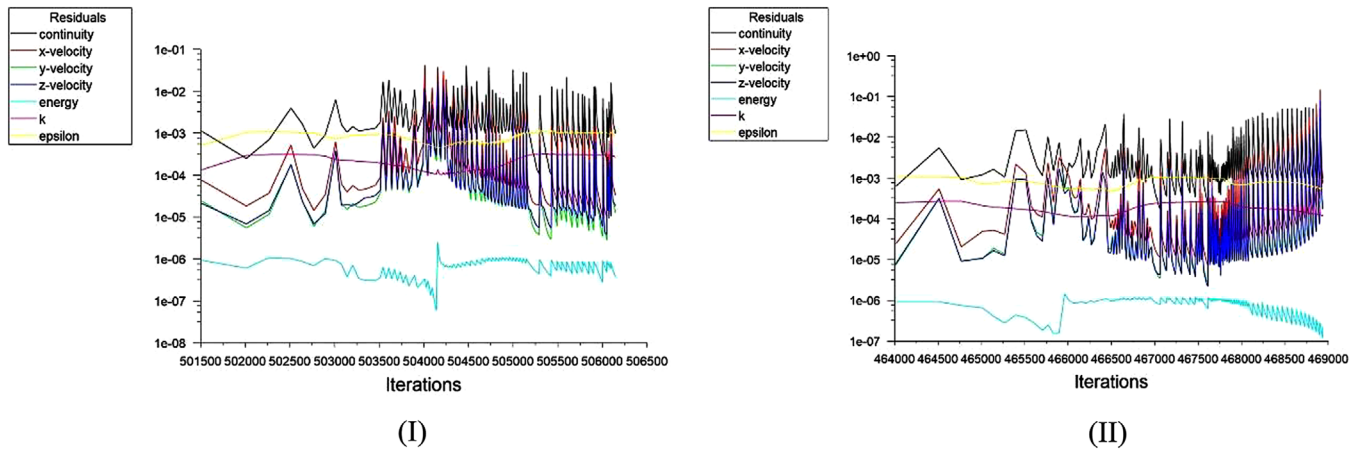


FIGURE 9 The convergence history for residuals. (I) Non-uniform inline regenerator. (II) Uniform inline regenerator

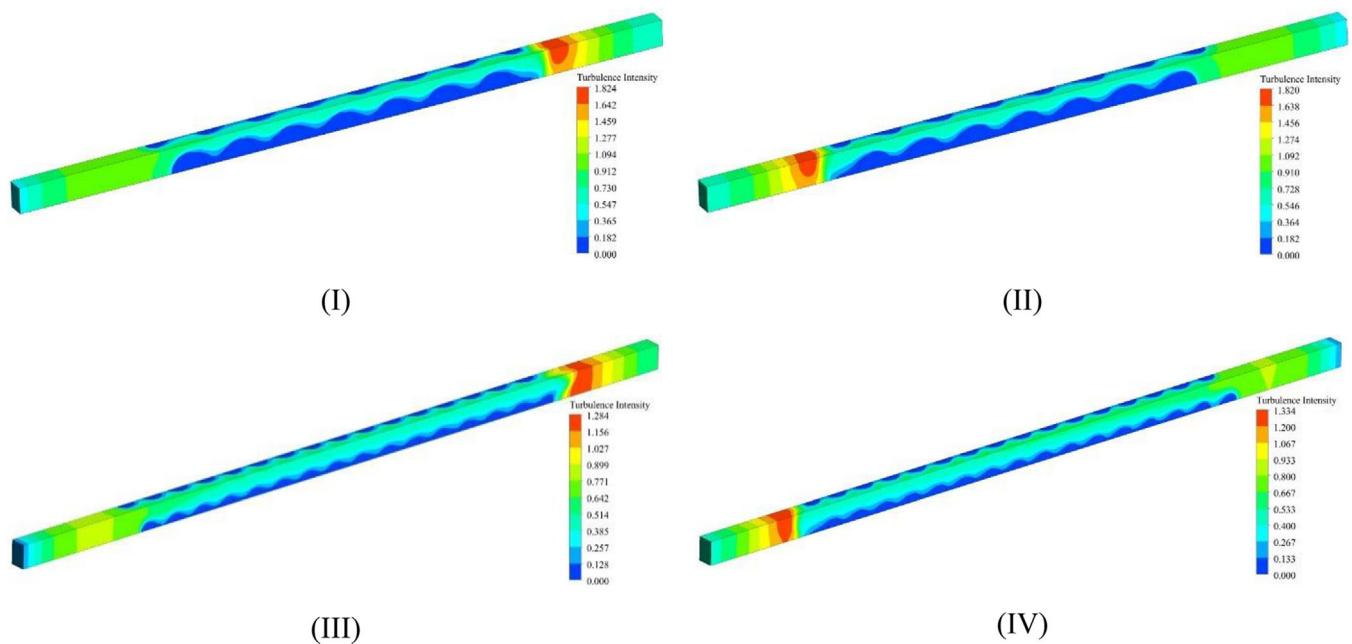
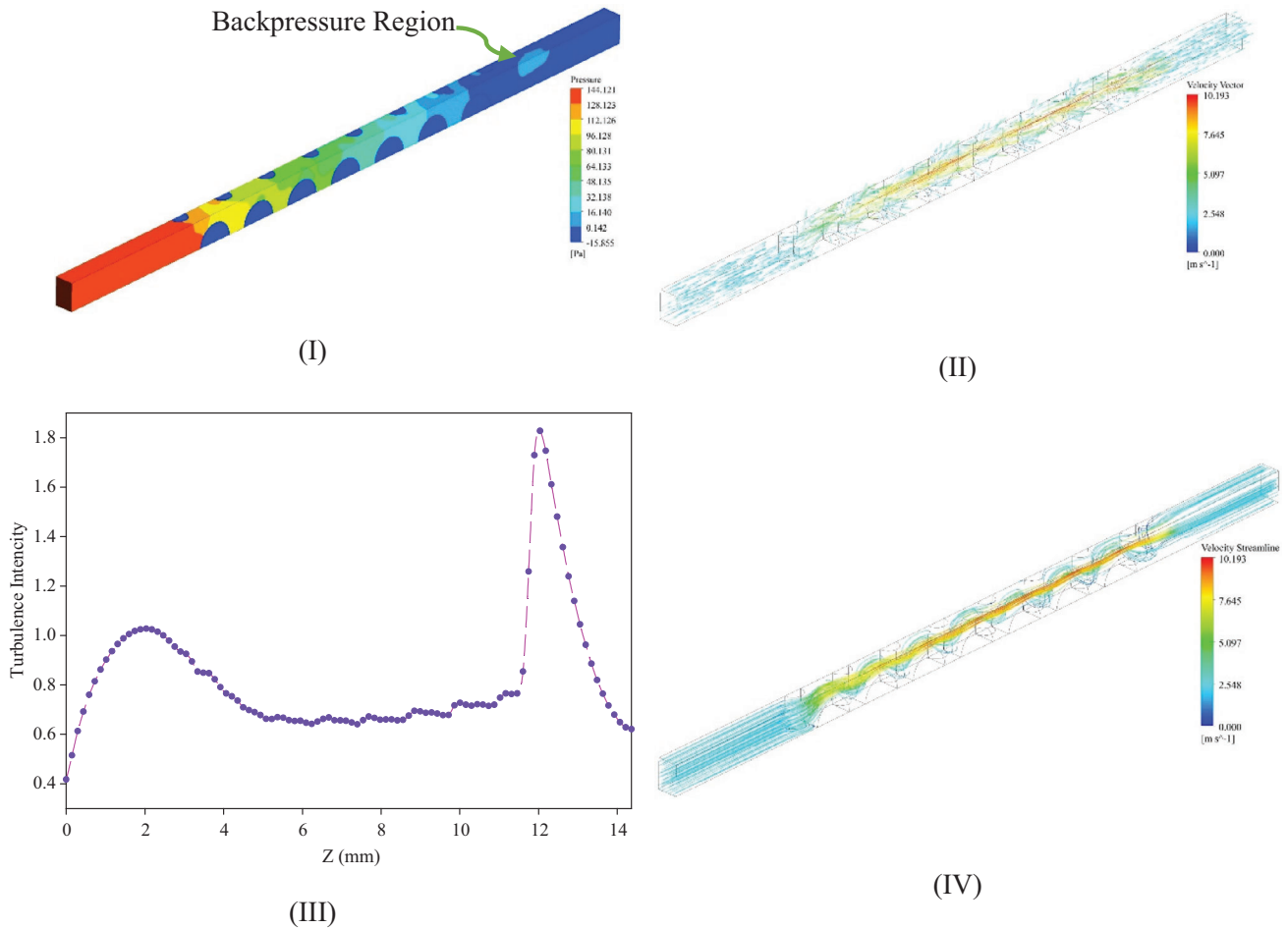


FIGURE 10 The turbulence intensity contour at  $\omega = 10$  rad/s and  $V_{\max} = 2$  m/s at flywheel angle  $\frac{\pi}{2}$  and  $\frac{3\pi}{2}$  in a heating and cooling period, respectively. (I) Heating period for non-uniform inline regenerator. (II) Cooling period for non-uniform inline regenerator. (III) Heating period for uniform inline regenerator. (IV) Cooling period for uniform inline regenerator

length, which can be attributed to its greater porosity of the packed bed. It is porosity of packed bed 1.45 times greater than uniform inline regenerator. Also, the uniform inline regenerator's matrix length is 1.45 times greater than the non-uniform inline regenerator ( $\frac{\varepsilon_I}{\varepsilon_{II}} = \frac{L_{II}}{L_I} = 1.45$ ). Therefore, for applications such as the Stirling engine, which has a spatial limitation of the regenerator installation, the non-uniform inline regenerator is recommended. The average thermal efficiency of non-uniform and uniform inline regenerators is approximately 85% and 80%, respectively. Hence, the non-uniform inline regenerator's average thermal efficiency is 5% higher than the uniform inline regenerator in the one period ( $2\pi$  flywheel angle). Temperature and velocity counters (Figures 6 and 8) show the trend

of changes instantaneously and cannot evaluate the regenerator's performance in the general state. However, by collecting data in a graph like Figure 7, it can be seen that the rate of pressure drop of the non-uniform is more than the uniform inline regenerator. Also, by averaging the graph, the average pressure drop of non-uniform and uniform inline regenerator is 76 and 61 Pa, respectively. Hence, the average pressure drop of the non-uniform inline regenerator is 15 Pa higher than the uniform inline regenerator in one period. The turbulence intensity is defined as follows:

$$I = \frac{\sqrt{\frac{2k}{3}}}{U} \quad (11)$$



**FIGURE 11**  $\omega = 10$  rad/s and  $V_{\max} = 2$  m/s at flywheel angle  $\frac{\pi}{2}$  and  $\frac{3\pi}{2}$  in a heating period for non-uniform inline regenerator. (I) Pressure contour. (II) Velocity vector contour. (III) Turbulence intensity as a Function of Streamwise Distance. (IV) Velocity streamline contour

Where  $I$ ,  $k$ , and  $U$  are turbulence intensity, turbulent kinetic energy, and mean velocity at the same location over the same time period, respectively. Large fluctuations in speed or direction in the unsteady flow can lead to more turbulence in the airflow, leading to turbulence intensity amount can be more than 1. Turbulence intensity contours for each of the heat regenerators are shown in Figure 10. In general, the turbulence intensity amount in the heating and cooling period in the non-uniform inline regenerator is more than the uniform inline regenerator. Also, after the airflow leaves the wires, the turbulence intensity value reaches its maximum. This sudden increase of turbulence intensity is accompanied by changes in the backpressure (Figure 11I) and velocity (Figure 11III,IV) contours. Also, Figure 11III gives turbulence intensity as a Function of Streamwise Distance along regenerator length. Maximum turbulence intensity occurs in the backpressure region with approximately 1.8. Moreover, the current study assumed **a** (inlet plane), **b** (middle plane), and **c** (outlet plane) according to Figure 2. Mean turbulence intensity value at the moment of airflow collision with the wire filaments in the heating (plane **a**) and cooling (plane **c**) period is greater than its value at the moment of the airflow leaving the woven wire screen in the heating (plane **c**) and cooling (plane **a**) period. In general, the mean turbulence intensity

in the middle length (plane **b**) of the regenerator has the lowest value, and its value is always  $\leq 0.2$ . Since we have the highest turbulence intensity in the inlet and outlet planes (**a**, **c**) of the regenerator, the maximum power loss and pressure drop occur in these zones. Therefore, it is better to use fluid flow conductors as stator blades at the inlet and outlet to reduce turbulence intensity in these regions.

## 6 | CONCLUSIONS

Woven metallic structure plays a significant role in heat return and increases thermal efficiency, among which inline regenerators are mostly used due to the simplicity of the structure. In the present study, by selecting two types of regenerators, only by changing the wires' diameter in a shorter length, approximately 5% average thermal efficiency was increased. Also, it imposes 15 Pa more mean pressure drop on the regenerator. Therefore, paying attention to the correct regenerator geometry as a critical factor in the inline regenerator is very important. Finally, the non-uniform inline regenerator is recommended for the Stirling engine, limiting the use of the regenerator length.



## ACKNOWLEDGEMENTS

This research was funded by the Teb Karan Aran Far Company, through the National Talent Sponsorship Contract (No. RS990431) of the corresponding author, which is highly acknowledged.

## NOMENCLATURE

$A$	Regenerator matrix heat transfer surface area, $m^2$
$A_c$	Cross-sectional area of the flow, $m^2$
$c_f$	Specific heat of flow at constant pressure, $J/kg\ K$
$d$	Wire diameter, $m$
$D_b$	Channel hydraulic diameter, $m$
$E$	Total energy, $J$
$f$	Friction factor
$G$	Gravity, $m/s^2$
$h$	Heat transfer coefficient, $W/m^2K$
$\vec{j}_j$	Diffusion flux of species $j$ , $kg/m^2s$
$k$	Thermal conductivity, $W/m\ K$
$k_{eff}$	Effective conductivity, $W/m\ K$
$k_t$	Turbulent thermal conductivity, $W/m\ K$
$L$	Regenerator length, $m$
$\dot{m}_f$	Mass flow rate, $kg/s$
$P$	Static pressure, $pa$
$\Delta P$	Pressure drop, $pa$
$Re$	Reynolds number
$T$	Temperature, $K$
$I$	Turbulence intensity
$t$	Time, $s$
$\vec{V}$	Overall velocity vector, $m/s$

## Greek symbols

$\varepsilon$	Porosity of packed bed
$\eta_{REG}$	Thermal efficiency
$\Lambda$	Reduced length
$\mu$	Absolute viscosity, $kg/m\ s$
$\rho$	Fluid density, $kg/m^3$
$\tau_{eff}$	Stress tensor, $pa$
$\omega$	Angular velocity, $rad/s$

## Subscripts

a	air
f	Fluid
h	Hot fluid
c	Cold fluid
in	Fluid entering
out	Fluid leaving
$x, y, z$	Cartesian coordinates




## CONFLICT OF INTEREST

The authors of the manuscript hereby declare that they have no conflict of interest.

## DATA AVAILABILITY STATEMENT

Data available on request due to privacy/ethical restrictions.

## ORCID

Hamed Mortazavi  <https://orcid.org/0000-0003-4218-2642>  
Hamidreza Mortazavy Beni  <https://orcid.org/0000-0002-6960-3251>  
Mohammad Saidul Islam  <https://orcid.org/0000-0001-6264-3886>

## REFERENCES

- Mortazavy Beni, H.: 3-D Numerical analysis of thermal/fluid characteristics of woven mesh structures as heat regenerators. M.S. thesis, Mechanical Engineering Department, Shiraz University, Iran (2007)
- Mortazavy Beni, H., Saranjam, B.: Stirling Engine. First edition, Malek-Ashtar University of Technology, Tehran, Iran (2009) ISBN: 978-964-8452-90-7.
- Mortazavy Beni, H.: Metallic Woven Mesh Structures to be used as Heat Regenerators. Patent No. A/85005186, Tehran, Iran (2010)
- Mortazavy Beni, H., Golneshan, A.A., Zarinchang, J.: 3-D Numerical analysis of thermal/fluid characteristics of woven mesh structures as heat regenerators. In: Proceedings of the 13th International Stirling Engine Conference, Germany, pp. 112–115 (2007)
- Tajdiny, A., Monsef, H., Lessani, H.: Optimized design of a novel yokeless mover permanent magnet linear generator for free-piston stirling engines applied to solar cogeneration systems. IET Renew. Power Gener. 15, 3631–3644 (2021)
- Tong, L.S., London, A.L.: Heat transfer and flow friction characteristics of woven-screen and cross-rod matrices. Trans. ASME 82(3), 1558–1570 (1957)
- Kays, W.M., London, A.L.: Compact Heat exchangers, 3rd Ed., McGraw-Hill, New York (1984)
- Xu, J., Wirtz, R.A.: In-plane effective thermal conductivity of plain-weave screen laminates. IEEE TCPT 25, 615–620 (2002)
- Park, J.-W., Ruch, D., Wirtz, R.A.: Thermal/fluid characteristics of isotropic plain-weave screen laminates as heat exchange surfaces. In: Proceedings of the AIAA Aerospace Sciences Meeting & Exhibit, Reno, NV (2002)
- Wirtz, R.A., Xu, J., Park, J.-W., Ruch, D.: Thermal/fluid characteristics of 3-D woven mesh structures as heat exchanger surfaces. IEEE Trans. Compon. Packag. Technol. 26(1), 40–47 (2003)
- Faruoli, M., Viggiano, A., Magi, V.: A porous media numerical approach for the simulation of stirling engine regenerators. TECNICA ITALIANA-Italian J. Eng. Science 63(2–4), 291–296 (2019)
- Mortazavy, H., Golneshan, A.A., Zarinchang, J.: 3-D Numerical Analysis of Thermal/Fluid Characteristics of Metallic Woven mesh Structures to be used as Heat Regenerators, M.S. Thesis, University of Shiraz, Iran (2007)
- Wilcox, D.C.: Turbulence Modeling for CFD, 2nd ed), DCW Industries, Inc, California (1994)
- Beni, H.M., Mortazavi, H.: Mathematical modeling of the solar regenerative heat exchanger under turbulent oscillating flow: Applications of renewable and sustainable energy and artificial heart. RINENG 13, 100321 (2022)
- Schmidt, F.W., John Willmott, A.: Thermal Energy Storage and Regeneration, Hemisphere Pub. Corp, Washington (1981)
- Conde, J.M.G., Pérez, M.A.S., Bravo, I.L.: GTER-dish, development of a dish-Stirling system model. SolarPACES Symposium, Granada, Spain (2011)
- Jaffe, L.D.: A review of test results on solar thermal power modules with dish-mounted Stirling and Brayton cycle engines. ASME J. Solar Energy Eng. 110(4), 268–274 (1988)
- Mancini, T., Heller, P., Butler, B., et al.: Dish-Stirling systems: An overview of development and status. Journal of Solar Energy Eng. 125, 135–151 (2003)
- Mortazavy Beni, H., Hassani, K., Khorramyeh, S.: Study of the sneezing effects on the real human upper airway using fluid–structure interaction method. J. Braz. Soc. Mech. Sci. Eng. 41, 181 (2019)
- Mortazavy Beni, H., Hassani, K., Khorramyeh, S.: In silico investigation of sneezing in a full real human upper airway using computational

- fluid dynamics method. *Comput. Methods Programs Biomed.* 177, 203–209 (2019)
21. Hamed, M., Mortazavy Beni, H., Aghaei, F., Sajadian, H.: SARS-CoV-2 droplet deposition path and its effects on the human upperairway in the oral inhalation. *Comput. Methods Programs Biomed.* 200(5448), 105843 (2020)
  22. Mortazavy Beni, H., Mortazavi, H., Aghaei, F., Kamalipour, S.: Experimental tracking and numerical mapping of novel coronavirus micro-droplet deposition through nasal inhalation in the human respiratory system. *Biomech Model Mechanobiol* 20(3), 1087–1100 (2021)
  23. Alaodolehei, B., Jafarian, K., Sheikhan, A., Mortazavy Beni, H.: Performance enhancement of an achalasia automatic detection system using ensemble empirical mode decomposition denoising method. *J. Med. Biol. Eng.* 40, 179–188 (2020)
  24. Babu, N.R., Saikia, L.C.: Load frequency control of a multi-area system incorporating realistic high-voltage direct current and dish-Stirling solar thermal system models under deregulated scenario. *IET Renew. Power Gener.* 15, 1116–1132 (2021)
  25. Khoshvaght-Aliabadi, M., Deldar, S., Salimi, A., Rashidi, M.M.: Effects of cross-section geometry on performance of corrugated miniature heat sink: Uniform, convergent, divergent, and hybrid cases, *Int. Commun. Heat Mass Transfer* 127, 105269 (2021)
  26. Khoshvaght-Aliabadi, M., Feizabadi, A., Nouri, M.: Design of novel geometries for minichannels to reduce junction temperature of heat sinks and enhance temperature uniformity. *Appl. Therm. Eng.* 192, 116926 (2021)
  27. Khoshvaght-Aliabadi, M., Soleimani, P., Rehman, S., Alimoradi, A.: Employing enhanced geometries in water bath heating system of natural gas pressure drop stations: Comparative study. *J. Nat. Gas Sci. Eng.* 87, 103775 (2021)

**How to cite this article:** Mortazavi, H., Mortazavy Beni, H., Islam, M.S.: Thermal/fluid characteristics of the inline stacked plain-weave screen as solar-powered Stirling engine heat regenerators. *IET Renew. Power Gener.* 16, 956–965 (2022).  
<https://doi.org/10.1049/rpg2.12405>